Variational reduced-density-matrix theory applied to the electronic structure of few-electron quantum dots

Adam E. Rothman and David A. Mazziotti*
Department of Chemistry and The James Franck Institute, The University of Chicago, Chicago, Illinois 60637, USA
(Received 13 May 2008; published 9 September 2008)

Variational two-electron reduced-density-matrix (2RDM) theory is applied to computing energy spectra and properties of few-electron quantum dots. The model system is a two-dimensional electron gas with a central confinement potential. For each orbital angular momentum J, the energy and 2RDM are computed by the variational 2RDM method in which the energy is minimized as a functional of the 2RDM. In the minimization, which is performed by semidefinite programming, the 2RDM is constrained to represent a N-electron wave function with angular momentum J by N- and J-representability conditions [D. A. Mazziotti, Phys. Rev. Lett. **93**, 213001 (2004)]. Advantages of the variational 2RDM method include (i) lower bounds on the energies for all J values, (ii) calculation of approximate 2RDMs in polynomial time without many-electron wave functions, (iii) exploitation of angular symmetry in the sparse block-diagonal structure of the 2RDM, (iv) accurate description of multireference correlation (entanglement) effects, and (v) direct calculation of one- and two-electron properties from the 2RDM. With the 2RDM we directly compute pair-correlation functions, radial charge densities, and average radial electron displacements in the quantum dot. Energies and properties are compared to those from solving the N-electron Schrödinger equation by large-scale, exact diagonalization. It is found that the accuracy of the variational 2RDM approach is sensitive to the total orbital angular momentum and the symmetry of the final wave function. For quantum dots of high symmetry, the variational algorithm isolates a highly accurate solution that recovers the correlation energy within a few percent.

DOI: 10.1103/PhysRevA.78.032510 PACS number(s): 31.10.+z

I. INTRODUCTION

Over the last quarter century, advances in semiconductor fabrication technology have facilitated the development of low-dimensional quantum structures. Depending on the dimensionality of the experimental setup, these structures are called quantum wells, wires, corrals, rings, or, more commonly, simply quantum dots. In broad terms, researchers create these structures by layering semiconducting materials of different Fermi energy in order to create a potential energy well. When the central layer is sufficiently thin, the quantized energy levels perpendicular to the layering (the z axis) are spaced so far apart that only the lowest state contains electronic population. As a result, electron motion is confined to the xy plane, with no freedom to move in the z direction. Confinement in fewer dimensions is achieved by application of external fields or by more complicated semiconductor layering schemes, creating potential energy wells in multiple dimensions [1].

Quantum dots are of fundamental interest in quantum chemistry and physics because they reveal exotic physical phenomena caused by electron correlation in low-dimensional environments. They demonstrate many of the same properties as atoms, including discrete spectra, shell structure, magnetization, etc., but on a much larger scale ($\sim$10–1000 nm). For this reason, quantum dots are sometimes referred to as "artificial atoms." In addition, the electronic properties of these dots are found to depend quite sensitively on their physical dimensions and externally applied fields, suggesting that future researchers may be able to tune the electronic spectrum of a quantum dot to suit a particular technological application. Specifically, many researchers are looking to quantum dots as a building block of a future generation of quantum computing devices [2–4].

In this paper, we study quantum dots formed by a two-dimensional electron gas subject to a magnetic field applied along the z axis. Motion in the z direction is neglected because the electron gas is strictly two dimensional. This model is meant to simulate physical quantum dots created by layered semiconductors, described above. In the xy plane, the wave function must tend to zero at infinite radius; rather than impose this condition as a hard constraint, we replace its effect by a force proportional to the distance from a central axis (i.e., a central parabolic potential). The behavior of one electron in this system was solved separately by Fock [5] and Darwin [6] in the early part of the twentieth century. However, the problem of electron-electron interactions in such a dot was not investigated until the end of the twentieth century, first by Maksym and Chakraborty [7–9] and subsequently by many others. Substantial effort has gone into the two-electron quantum dot ("quantum-dot helium"), with the research focus on Hartree-Fock [10], perturbation [11], variational [12,13], discrete-variable representation [14], and exact-diagonalization [configuration-interaction (CI)] theories [15]. Other authors have investigated particular analytical solutions for this system, typically by approximating the interelectronic potential [16,17]. For more than two electrons, research efforts have focused on quantum Monte Carlo studies [18,19], density-functional theories [20], and CI [21,22]. Although CI is the most universal of these methods, the large number of one-particle basis functions required to describe the dot makes it intractable for more than about ten electrons. For interacting, N-electron quantum dots, total or-

*damazz@uchicago.edu

bital angular momentum $J=\Sigma_{i=1}^{N} l_i$ is a good quantum number, and a different electronic ground state may be identified for each value of J.

Whenever an atomic or molecular Hamiltonian may be expressed as the sum of one- and two-body interactions, the indistinguishability of the electrons permits us to express the energy as a linear functional of the two-electron reduced density matrix (2RDM). In these cases, the full N-particle wave function of the system contains too much information if only energies and one- and two-body properties of the system are desired. For this reason, quantum chemists and physicists have devoted substantial research to the direct calculation of 2RDMs. Unfortunately, research stalled in this arena for fifty years because the 2RDM must be constrained to ensure it corresponds to a N-electron quantum system. The necessary constraints are known as N-representability conditions. Two general approaches to the direct calculation for the 2RDM have recently been developed [23]: (i) the nonvariational solution of the anti-Hermitian contracted Schrödinger equation (ACSE) by cumulant reconstruction of the three-particle reduced density matrix [24–34] and (ii) the variational calculation of the 2RDM by performing constrained minimization of the system energy [35–40]. The N-representability conditions enforce the physical properties of N-electron wave functions on a two-electron RDM; without them, the variational minimization [approach (ii)] would yield an energy well below the true ground-state energy.

Both categories of 2RDM calculations are mathematically rigorous and capable of calculating accurate ground-state energies of atoms and molecules [26,41,42]. In this paper, we apply the variational RDM framework to interacting quantum dots. The RDM formalism is an ideal approach to the calculation of energies and properties of interacting quantum dots for several reasons. First, for many values of total orbital angular momentum J, the interacting dots are highly correlated systems—dramatically more correlated than their molecular counterparts. In these cases, the absence of a specific reference determinant in 2RDM theory means we should be able to capture essential, multireference effects without resorting to expensive, multireference calculations [39,43]. Partly as a result of the high correlation in these systems, the number of single-electron basis functions needed to describe a dot is typically greater than the number of functions needed for a molecule of comparable size (i.e., number of electrons)—particularly as J increases. Thus, the improved scaling of RDM methods over CI will be particularly significant in large-scale calculations [39]. Moreover, the high rotational symmetry of the quantum dot (reflected in the importance of J) imposes a sparse block structure on two- and higher-particle RDMs that facilitates their calculation.

The remainder of the paper is organized as follows. Section II presents the quantum-dot model Hamiltonian in detail, with specific emphasis on the role of total orbital angular momentum. The section continues by reviewing the key concepts of variational RDM theory, including a brief recount of two- and three-particle N-representability conditions. We develop a special set of N-representability conditions, called J-representability conditions, that constrain the 2RDM to represent a many-electron wave function with a specific value of the total angular momentum operator $\hat{J}$. Section III lays out computational details, including unique symmetries implicit in the quantum-dot Hamiltonian that facilitate our calculations. Section IV presents the energies and selected properties of few-electron quantum dots calculated by the variational minimization procedure and compares them to the configuration-interaction solution. The results are discussed in light of what is known about the properties of wave functions in interacting quantum dots. Finally, in Sec. V we comment on the efficacy of 2RDMs in quantum dot electronic structure calculations.

II. THEORY

A. Model quantum dot hamiltonian and single-electron basis functions

Following the literature [7,9,44], we consider the motion of one electron in a two-dimensional circular dot, confined by a parabolic potential $\frac{1}{2}m^*\omega_0^2 r^2$ and in the presence of an externally applied, perpendicular magnetic field $\mathbf{B}=(0,0,B)$. The parameter m^* is the electron's effective mass, which is taken as a constant for a given semiconductor background. In this system, individual electrons are described by the Hamiltonian

$$\hat{h}_1 = \frac{1}{2m^*}\left(\mathbf{p} - \frac{e}{c}\mathbf{A}\right)^2 + \frac{1}{2}m^*\omega_0^2|\mathbf{r}|^2. \tag{1}$$

Choosing the symmetric gauge vector potential $\mathbf{A}=\frac{B}{2}(-y,x,0)$, the one-electron Hamiltonian has been solved [5,6] to yield the one-particle energies

$$E_{n,l} = (2n+|l|+1)\Omega - \frac{1}{2}\omega_c l, \tag{2}$$

where the cyclotron frequency and the effective confinement frequency are $\omega_c=eB/(m^*c)$ and $\Omega^2=\omega_0^2+\omega_c^2/4$, respectively. In atomic units ($\hbar=m_e=e=1$), the normalized, single-particle wave functions are

$$|n,l\rangle \equiv \psi_{n,l}(\mathbf{r}) = \frac{1}{\sqrt{2\pi}\Lambda}\left[\frac{n!}{(n+|l|)!}\right]^{1/2} \times e^{-il\theta}\left(\frac{r}{\sqrt{2}\Lambda}\right)^{|l|}\exp\left(\frac{-r^2}{4\Lambda^2}\right)L_n^{|l|}\left(\frac{r^2}{2\Lambda^2}\right), \tag{3}$$

where $L_n^{|l|}$ is an associated Laguerre polynomial and the parameter Λ is a natural length scale for the quantum dot, given by $\Lambda^2=1/(2m^*\Omega)$. These basis functions are orthonormal and are eigenfunctions of the azimuthal angular momentum operator

$$\hat{L}_z|n,l\rangle = i\frac{\partial}{\partial\theta}|n,l\rangle = l|n,l\rangle, \tag{4}$$

which, as we will show, has important consequences for the dot's many-electron physics.

Each eigenfunction depends on two quantum numbers: a radial quantum number $n=0,1,\ldots$, and an azimuthal quan-

tum number $l=0,\pm1,\pm2,\ldots$. Since the dot is a two-dimensional system, the angular-momentum-squared operator $\hat{\mathbf{L}}^2$ reduces to $\hat{L}_z^2$. Unlike hydrogenic orbitals, the absolute value of the azimuthal quantum number may exceed the radial quantum number. Observe that $\Omega \geqslant \omega_c/2$, but for large B or small confinement potential this inequality approaches equality. Thus, the single-particle energies [see Eq. (2)] form bands separated by about $\hbar\omega_c$ around each value of n [i.e., $(n+\frac{1}{2})\hbar\omega_c$], with individual energy levels increasing with positive l; states with $l<0$ have much greater energies and lie in higher bands. These bands are called Landau levels [45] or Fock-Darwin levels [44], where each band is labeled by a Fock-Darwin index $\mathcal{N}_{\mathrm{FD}}=n+\frac{l-|l|}{2}$. It will be shown in Sec. III that the band structure of the one-electron energies becomes a convenient means to truncate the one-electron basis functions for electronic structure calculations.

With the motion of one electron under parabolic confinement understood, we turn to considering the behavior of multiple electrons subject to the same potential and a modified, two-dimensional Coulomb-type repulsion. Although the magnetic field imposes an energy difference between α and β electrons, following the literature [7] we assume in this work that the field is strong enough to overwhelm the splitting energy and spin polarize all electrons to one spin or the other. This stipulation negates the need to include the spin-splitting energy or the effect of spin-spin coupling in the many-electron Hamiltonian because either term would only add a constant contribution to the overall energy. By additionally neglecting spin-orbit interactions, we render our model essentially spinless; since we do not allow the electrons' spin to couple to each other or to the orbital angular momentum, spin is effectively removed from the many-electron system. Explicitly separating out the contribution of the angular momentum, the N-electron interacting Hamiltonian is (in atomic units)

$$\hat{\mathcal{H}} = \sum_{i=1}^{N}\left[\frac{\hat{\mathbf{p}}_i^2}{2m^*} + \frac{m^*\Omega^2}{2}\mathbf{r}_i^2\right] + \sum_{i<j}\frac{1}{\epsilon|\mathbf{r}_i-\mathbf{r}_j|} - \sum_{i=1}^{N}\frac{\omega_c}{2}\hat{L}_{z,i}, \tag{5}$$

where ϵ describes the dielectric constant of the underlying semiconductor substrate.

Equation (5) makes clear the importance of angular momentum to the N-electron system. Because $\hat{\mathcal{H}}$ commutes with $\hat{J}=\Sigma_i\hat{L}_{z,i}$, each N-electron wave function is labeled by a total angular momentum quantum number J, meaning wave functions with different values of J do not mix. Therefore, we may piece together the total spectrum of $\hat{\mathcal{H}}$ by examining each J individually. Quantum-dot CI calculations exploit the angular momentum quantum number by truncating the interaction matrix to only Slater determinants consistent with a predetermined value of J [44]. Implementing a similar restriction from an RDM perspective is more difficult because Slater determinants are not a part of the theory; in fact, a strict variational minimization of Eq. (5) will result in an energy minimum regardless of J. Instead, the variational procedure must constrain the 2RDM to yield a specific value of J. In Sec. III, we will develop constraints to enforce a physical behavior from ${}^2D$ with respect to the total angular momentum operator $\hat{J}$. We call these constraints J-representability conditions. However, even when calculations are conducted in J subspaces of the total Hamiltonian, it is important to remember that compared to the overall ground state for a given number of particles (which occurs at a single angular momentum value), electronic ground states at higher angular momentum are still essentially excited states of the quantum dot.

In order to facilitate the discussion in Sec. II B regarding variational RDM mechanics, we reformulate the quantum-dot Hamiltonian in second quantization. Introducing the standard creation (annihilation) operators $\hat{a}_{n,l}^\dagger$ ($\hat{a}_{n,l}$), which create (destroy) an electron with quantum numbers n and l, we may write the many-electron Hamiltonian as

$$\hat{\mathcal{H}} = \sum_p E_p\hat{a}_p^\dagger\hat{a}_p + \sum_{p,q,s,t} V_{st}^{pq}\hat{a}_p^\dagger\hat{a}_q^\dagger\hat{a}_t\hat{a}_s, \tag{6}$$

where the composite index $p=(n,l)$ (similarly q,s,t) denotes the two quantum numbers for the one-electron wave functions in Eq. (3). The first term in Eq. (6) accounts for the one-electron energies E_p given by Eq. (2), and the electron-electron interaction matrix elements are

$$V_{st}^{pq} = \frac{1}{2\epsilon}\langle pq|st\rangle = \delta_{l_p+l_q,l_s+l_t}\frac{1}{2\epsilon}\int d\mathbf{r}_1 d\mathbf{r}_2\psi_p^*(\mathbf{r}_1)\psi_q^*(\mathbf{r}_2)\frac{1}{|\mathbf{r}_1-\mathbf{r}_2|}\psi_s(\mathbf{r}_1)\psi_t(\mathbf{r}_2), \tag{7}$$

where the Krönecker delta function over the angular-momentum quantum numbers is a mathematical manifestation of angular-momentum conservation between two electrons in the two-center integral. The delta function also ensures that the phases from each one-electron wave function cancel exactly, leaving the resulting integral purely real. In the second-quantized notation, the important total orbital angular momentum operator is $\hat{J}=\Sigma_i\hat{L}_{z,i}=\Sigma_i l_i\hat{a}_i^\dagger\hat{a}_i$. With these definitions and the fermionic anticommutation relations, it is easy to verify that $[\hat{J},\hat{\mathcal{H}}]=0$.

B. Variational 2RDM theory

Because the quantum-dot Hamiltonian contains at most pairwise interactions, the energy of an N-electron dot with ground-state wave function $|\Psi\rangle$ may be expressed as a linear functional of the 2RDM

$$E = \sum_{p,q,s,t}{}^2K_{st}^{pq}\langle\Psi|\hat{a}_p^\dagger\hat{a}_q^\dagger\hat{a}_t\hat{a}_s|\Psi\rangle = \mathrm{Tr}({}^2K^2D), \tag{8}$$

where the two-electron reduced Hamiltonian is given by

$${}^2K_{st}^{pq} = \frac{1}{N-1}(\delta_s^p\langle q|\hat{h}_1|t\rangle + \delta_t^q\langle p|\hat{h}_1|s\rangle) + V_{st}^{pq}. \tag{9}$$

Equation (8) suggests that the ground-state energy may be obtained by straightforward minimization with respect to the 2RDM. However, since the set of all 2RDMs is bigger than

the set of 2RDMs derivable from physical, N-electron wave functions, unconstrained minimization of Eq. (8) will yield an energy well below the true ground-state energy [23,46–48]. Thus, N-representability constraints must be imposed on the minimization to ensure the resulting 2RDM corresponds to a physical N-electron wave function.

1. N-representability conditions

In addition to the standard conditions for a matrix to be a fermionic density matrix [48,49], p-positivity conditions $1 \leqslant p \leqslant N$ constitute an important class of N-representability constraints [23,48,50–52]. The positivity conditions are a hierarchy of constraints that enforce the generalized uncertainty relations for all pairs of operators with $p/2$-body interactions [51]. They are implemented by constructing the metric (overlap) matrices

$$M_j^i = \langle \Psi | \hat{C}_i^\dagger \hat{C}_j | \Psi \rangle \tag{10}$$

and constraining them to be positive semidefinite (i.e., all eigenvalues non-negative, denoted $M \geqslant 0$). Full p-positivity is enforced by choosing the operators $\hat{C}_i$ to be all products of p one-electron creation and/or annihilation operators.

In particular, by choosing the operators $\hat{C}_i$ from the set of all combinations of three creation and/or annihilation operators, we generate the three-positivity conditions [23,51,52]:

$${}^3D_{lmn}^{ijk} = \langle \Psi | \hat{a}_i^\dagger \hat{a}_j^\dagger \hat{a}_k^\dagger \hat{a}_n \hat{a}_m \hat{a}_l | \Psi \rangle, \tag{11a}$$

$${}^3E_{lmn}^{ijk} = \langle \Psi | \hat{a}_i^\dagger \hat{a}_j^\dagger \hat{a}_k \hat{a}_n^\dagger \hat{a}_m \hat{a}_l | \Psi \rangle, \tag{11b}$$

$${}^3F_{lmn}^{ijk} = \langle \Psi | \hat{a}_i \hat{a}_j \hat{a}_k^\dagger \hat{a}_n \hat{a}_m^\dagger \hat{a}_l^\dagger | \Psi \rangle, \tag{11c}$$

$${}^3Q_{lmn}^{ijk} = \langle \Psi | \hat{a}_i \hat{a}_j \hat{a}_k \hat{a}_n^\dagger \hat{a}_m^\dagger \hat{a}_l^\dagger | \Psi \rangle, \tag{11d}$$

where ${}^3D \geqslant 0$, ${}^3E \geqslant 0$, ${}^3F \geqslant 0$, and ${}^3Q \geqslant 0$. Physically, the positivity of these matrices ensures that the probability distributions of finding three electrons (^3D), two electrons and a hole (^3E), one electron and two holes (^3F), or three holes (^3Q), are everywhere non-negative. These matrices may be mapped onto one another by rearranging the creation and annihilation operators in accord with the fermionic anticommutation relations [53]. However, since each matrix has a distinct physical meaning, the positivity of one matrix does not imply the positivity of the other three matrices.

By identifying the number operator $\hat{N} = \Sigma_i \hat{a}_i^\dagger \hat{a}_i$ within each of the matrices defined in Eqs. (11), the three-positivity conditions imply the two-positivity conditions [35,36,50]:

$${}^2D_{kl}^{ij} = \langle \Psi | \hat{a}_i^\dagger \hat{a}_j^\dagger \hat{a}_l \hat{a}_k | \Psi \rangle, \tag{12a}$$

$${}^2Q_{kl}^{ij} = \langle \Psi | \hat{a}_i \hat{a}_j \hat{a}_l^\dagger \hat{a}_k^\dagger | \Psi \rangle, \tag{12b}$$

$${}^2G_{kl}^{ij} = \langle \Psi | \hat{a}_i^\dagger \hat{a}_j \hat{a}_l^\dagger \hat{a}_k | \Psi \rangle, \tag{12c}$$

which, in turn, imply the one-positivity conditions

$${}^1D_j^i = \langle \Psi | \hat{a}_i^\dagger \hat{a}_j | \Psi \rangle, \tag{13a}$$

$${}^1Q_j^i = \langle \Psi | \hat{a}_i \hat{a}_j^\dagger | \Psi \rangle. \tag{13b}$$

The positivity of these matrices has an analogous physical interpretation as the three-positivity matrices, but on the space of two [or one, in the case of Eqs. (13)] electrons and/or holes. Because the positivity constraints are necessary N-representability conditions, variational minimization of the ground-state energy with respect to a 2RDM restricted by these constraints yields a lower bound [23,48,50–52]. As shown in the next section, such a lower bound can be calculated for the ground-state energy of each symmetry class, where for quantum dots these classes correspond to different values of the orbital angular momentum.

2. J-representability conditions

Because the quantum-dot Hamiltonian commutes with the total orbital angular momentum operator $\hat{J}$, each solution to the Schrödinger equation (i.e., each ^2D) corresponds to an integer value of J. Therefore we may compute energy spectra for a quantum dot by determining the N-representable minimum of Eq. (8) for each J. However, straightforward minimization of Eq. (8), even when constrained by the positivity conditions described above, does not yield an integer value of J. To make the variationally determined 2RDM physically meaningful, we must add necessary conditions on each 2RDM that constrain its underlying wave function to be an eigenfunction of angular momentum operator $\hat{J}$ with specific J quantum number. With a knowledge of the 2RDM we can enforce the trace condition

$$J = \langle \Psi | \hat{J} | \Psi \rangle = \sum_i l_i {}^1D_i^i \tag{14}$$

and the contracted Schrödinger equation [28,30,32]

$$\langle \Psi | \hat{a}_i^\dagger \hat{a}_j \hat{J} | \Psi \rangle = J \, {}^1D_j^i, \tag{15}$$

for the one-body Hamiltonian $\hat{J}$. The contracted Schrödinger equation with the trace condition in Eq. (14) implies the dispersion condition [32,54]

$$\langle \Psi | (\hat{J} - J)^2 | \Psi \rangle = 0. \tag{16}$$

In the presence of necessary and sufficient N-representability conditions the contracted Schrödinger equation plus the trace condition is equivalent to the dispersion condition, which becomes a necessary and sufficient J-representability constraint [30,32]. In the absence of complete N-representability conditions, however, the contracted Schrödinger equation is a more stringent J-representability constraint than the dispersion condition [51]. If ${}^3D$ is also available, we can enforce the more general contracted Schrödinger equation [33]

$$\langle \psi | \hat{a}_i^\dagger \hat{a}_j \hat{a}_k^\dagger \hat{a}_l \hat{J} | \Psi \rangle = J \, {}^2G_{lk}^{ij}, \tag{17}$$

whose second-quantized operators can be rearranged to obtain a sum over the matrix elements of ${}^3D$.

III. COMPUTATIONAL DETAILS

Since the single-particle quantum-dot basis functions in Eq. (3) are not hydrogenic orbitals, the litany of standard

quantum-chemical basis sets (e.g., STO, Dunning-Hay, double-zeta, etc.) is not helpful in selecting the appropriate number of one-electron basis functions for a quantum dot with N electrons and total orbital angular momentum J. The literature employs two different strategies for this procedure: (i) including all basis functions with one-particle energies less than a predetermined cutoff [22] or (ii) selecting a maximum Fock-Darwin index $\mathcal{N}_{\text{tot}}$ and then forming a basis from all states $|n,l\rangle$ that may combine to form N-electron Slater determinants with the desired J and total Fock-Darwin index $\Sigma_{i=1}^{N}(\mathcal{N}_{\text{FD}})_i \leqslant \mathcal{N}_{\text{tot}}$ [44]. With either prescription, the total Fock-Darwin index is not a good quantum number, but rather a convenient means of selecting basis states. We chose the latter approach because it is less arbitrary and reflects the energy band structure of electrons under parabolic confinement. CI calculations reveal that this means of truncating the one-electron space, with typical $\mathcal{N}_{\text{tot}}=1$, yields energies within a few percent of the infinite-basis energy.

For energy comparisons, uncorrelated (Hartree-Fock) energies are obtained via a self-consistent field procedure constrained to ensure the reference determinant is of the proper angular momentum J [55,56]. Exact energies are obtained by a full CI procedure within the given basis that first sorts the interaction matrix by total angular momentum J and then only diagonalizes the block corresponding to the angular momentum of interest.

Calculating properties of the quantum dot systems is accomplished by taking the trace of property matrices against the one- and two-particle RDMs [46]. For the variational RDM calculations, this procedure is particularly simple because the theory results in an optimized density matrix. For both Hartree-Fock and CI calculations, the 2RDM is first constructed from the wave function by integration (or contraction) [47], and then used to calculate all desired properties.

A. Spin and symmetry considerations

Since our model quantum dot contains electrons of only one spin or the other, the various N-representability conditions we employ are simpler than earlier work [36,57] because each metric matrix in the positivity conditions contains only one spin block. Furthermore, even through the typical quantum-dot one-electron bases are far larger than their atomic and molecular counterparts for a given number of electrons, the high rotational symmetry of the dot enforces a rigorous block-diagonal structure on all reduced density matrices, which dramatically shrinks the number of nonzero elements.

Consider an individual matrix element of ${}^2D$, defined in Eq. (12a). We know the system wave function $|\Psi\rangle$ is labeled by a total orbital angular momentum quantum number J and that wave functions corresponding to different values of J are orthogonal. If $l_i+l_j-l_k-l_l\neq 0$, the ket obtained by acting to the right with all the creation and annihilation operators will have a different J than the bra $\langle\Psi|$, producing a zero matrix element. Therefore, the ${}^2D$ and ${}^2Q$ forms of the 2RDM obey the block diagonal structure $l_i+l_j=l_k+l_l$, while the metric matrix ${}^2G$ obeys the slightly different condition $l_i-l_j=l_k-l_l$. Physically, these conditions reflect conservation of angular momentum between the particles created and/or destroyed by the creation and annihilation operators in the definition of each RDM. Similar relationships may be identified for each of the 1RDMs and 3RDMs.

The angular momentum symmetry of the dot also gives rise to a special type of J-representability condition. Consider an individual Slater determinant in the wave function. Naturally the sum of all N angular momenta in the determinant is J; however, it is also instructive to break up the sum into two components

$$\underbrace{l_1+\cdots+l_p}_{p\ \text{terms}}+\underbrace{l_{p+1}+\cdots+l_N}_{N-p\ \text{terms}}=J. \tag{18}$$

In other words, for a given J, knowledge of the sum of p of the N angular momenta determines the sum of the remaining $N-p$ momenta, or vise versa. This relationship is useful in the context of RDMs because each p-RDM is the result of integrating over $N-p$ particles from the full density matrix [46,47]. Generalizing Eq. (18) from an individual Slater determinant to the complete wave function yields the relationship

$$\text{Tr}({}^pD_l)=\text{Tr}({}^{N-p}D_{J-l}), \tag{19}$$

where the right subscript indicates a specific angular momentum block of the RDM. When at least $N/2$-positivity conditions are employed, Eq. (19) enforces an important angular momentum condition on the variationally determined RDMs.

B. Summary of N-representability conditions

All constrained variational minimizations are performed using the first-order, nonlinear algorithm for semidefinite programming developed by Mazziotti [38,39]. Computational cost of the variational 2RDM calculation without angular symmetry scales as r^6 for two-positivity constraints and r^9 for three-positivity constraints where r is the number of one-electron basis functions [39]. With the sparsity of the metric matrices from angular symmetry the cost is considerably less. The following N-representability conditions are employed to generate the results in Sec. IV.

(1) The antisymmetry of 2RDM indices

$${}^2D_{kl}^{ij}=-{}^2D_{kl}^{ji}=-{}^2D_{lk}^{ij}={}^2D_{lk}^{ji} \tag{20}$$

is automatically enforced by using the antisymmetrized basis functions $\tilde{\phi}_{ij}=(\phi_{ij}-\phi_{ji})/\sqrt{2}\ \ \forall j<i$. Analogous antisymmetrized basis functions are used for higher RDMs.

(2) The trace condition

$$\frac{N(N-1)}{2}=\sum_{i>j}{}^2D_{ij}^{ij}. \tag{21}$$

(3) The contraction condition(s)

$$(N-1)\,{}^1D_j^i=\sum_k {}^2D_{jk}^{ik},$$

$$(N-2)\,{}^2D_{kl}^{ij}=\sum_n {}^3D_{kln}^{ijn}. \tag{22}$$

(4) Each RDM, constrained to be Hermitian, is blocked by angular momentum.

(5) Positivity conditions are applied to all RDMs. In particular, ${}^1D \geqslant 0$, ${}^1Q \geqslant 0$, ${}^2D \geqslant 0$, ${}^2Q \geqslant 0$, and ${}^2G \geqslant 0$. Where indicated, we also require ${}^3D \geqslant 0$ and/or ${}^3Q \geqslant 0$.

(6) The different RDMs are related by linear mappings which stem from the fermionic anticommutation relations.

(7) To impose J representability, the 1RDM is always constrained by the trace condition in Eq. (14) and the contracted Schrödinger condition in Eq. (15). If the 3RDM is available as in a calculation with partial three-positivity conditions, we enforce the more general contracted Schrödinger condition in Eq. (17).

Finally, our calculations indicate that for small numbers of electrons ($N=4-6$), constraining the traces of individual blocks of ${}^2D$ and ${}^3D$ in accord with Eq. (19) improves the computed result. However, to maintain generality for larger numbers of electrons (where the order of the density matrices is not large enough to employ trace matching), we omit this constraint from the calculations shown here.

IV. NUMERICAL RESULTS AND DISCUSSION

We used variational RDM theory to investigate the ground-state energy and rudimentary properties of N-electron quantum dots ($N \leqslant 8$) for a variety of total orbital angular momenta J. The variational results are compared to Hartree-Fock theory and the exact result (CI) within the given basis. The range of angular momenta studied varies for each number of particles because additional particles increase the ground-state angular momentum [e.g., in the lowest Fock-Darwin level $\mathcal{N}_{\text{tot}}=0$, the smallest possible angular momentum for N particles is $J=0+1+2+\cdots+N-1=N(N-1)/2$]. We choose the model parameters to emulate a GaAs quantum dot $m^*=0.067m_e$, $\omega_0=4.0$ meV, $\epsilon=12.4$. Simulations were conducted both at $B=2$ T and $B=10$ T to recreate low- and high-magnetic field behavior. Single-particle basis sets were constructed in accord with our description in Sec. III using a total Fock-Darwin index cutoff $\mathcal{N}_{\text{tot}}=1$.

The ground-state energy spectra for four electrons at both low ($B=2.0$ T) and high ($B=10.0$ T) magnetic fields are displayed in Fig. 1. The spectra show the Hartree-Fock energy (denoted HF), exact diagonalization energy (denoted FCI) and the calculated energy from the variational RDM calculation (denoted DQG or D3, depending on the strength of the positivity conditions employed). We present this system first because (i) it is small enough so that we may perform calculations at many different values of J and (ii) the results for four electrons are generally indicative of systems with more electrons where computational considerations prevent tabulation of large quantities of data.

In general, the ground-state energy increases with J for the simple reason that the one-electron energy [see Eq. (2)] increases with l. However, the magnetic field strength affects at which J the overall ground state occurs. At low fields, the ground state is the smallest J compatible with placing all electrons in the lowest Fock-Darwin level $\mathcal{N}_{\text{FD}}=0$; thus the ground state for four electrons at low field is $J=6$. At higher fields, the competition between the single-electron energies and the interaction energy leads to a ground-state angular momentum at a higher J value [44]. This explains the competing energy behaviors between Figs. 1(a) and 1(b).

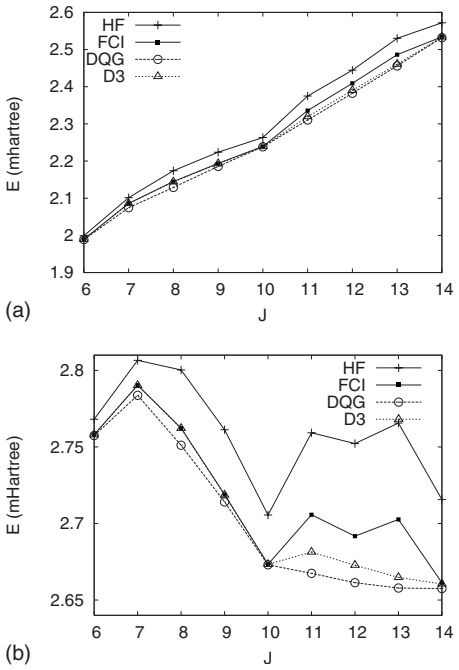

FIG. 1. Energy spectrum as a function of J for four electrons at (a) $B=2.0$ T and (b) $B=10.0$ T at the Hartree-Fock (HF), exact diagonalization (FCI), two-positive RDM (DQG) and partial three-positive RDM (D3) levels of theory. The magnetic field alters the overall ground state of the dot, leading to different behavior with J in each case. It is seen that both levels of variational RDM theory yield very accurate energies for the magic angular momenta $J=6$, 10, and 14. Away from these values, applying the stronger D3 condition improves the variationally determined energy.

More importantly, the spectra in Fig. 1 exhibit cusps (or local minima) in the energy spectrum at special values of J. For four electrons, these magic values of angular momenta occur at $J=6,10,14$ (for five electrons, see $J=10,15$ in Fig. 4). The exact origin of magic angular momenta states is a combination of the electronic exchange interaction and symmetry considerations [58–60]. In the simplest model, electrons minimize their Coulombic repulsion by attaining maximal angular separation at a fixed radius; in other words, the electron density is localized about the vertices of a N-sided polygon. In these configurations, certain cyclic permutations of the electrons are equivalent to rotations generated by the azimuthal angular momentum operator $\hat{L}_z$. By the Pauli principle, these low-energy configurations can only occur at the magic angular momenta values, given by $J_m=N(N-1)/2+kN$ for integer k. For larger numbers of electrons, alternate magic angular momenta series exist, formed by localizing n of N electrons at the center of the dot ($n/N \ll 1$; typically $n=1$) and arranging the remaining electrons in a polygon with $N-n$ vertexes [59].

The magic numbers are significant in the context of variational RDM theory because the accuracy of the constrained minimization procedure (compared to the exact energy) is found to depend on whether a given system is in a "magic"

TABLE I. Occupation numbers of the natural orbitals for four electrons at $B=2.0$ T for several different values of J. Although correlation generally increases with J, the magic angular momenta states (bold) are noticeably less correlated than their nonmagic counterparts. The natural orbitals are the eigenfunctions of the 1RDM.

	CI occupation numbers of natural orbitals					
Orbital	$J=$**6**	8	**10**	12	**14**	16
1	0.9956	0.9833	0.9613	0.7488	0.8157	0.6115
2	0.9911	0.9790	0.9297	0.7360	0.7863	0.5573
3	0.9851	0.6207	0.8368	0.6469	0.6989	0.4849
4	0.9816	0.6199	0.7510	0.5811	0.6249	0.4686
5	0.0164	0.3830	0.2488	0.4742	0.3657	0.4625

state. For the four-electron dot, full two-positivity (denoted DQG) captures about 106% of the correlation energy at both low- and high-magnetic fields (by definition, the Hartree-Fock energy captures 0% of the correlation energy while the exact answer recovers 100% of the correlation energy). At nonmagic J values, the constrained RDM minimization does not perform as well. On the first magic period ($6<J<10$), the DQG procedure recovers an average of 151% of correlation at low field and 127% of correlation at high field. The accuracy drops to an average of 161% of correlation at low magnetic field and 164% of correlation at high field over the second magic period ($10<J<14$). The data prompt the important question of why the variational RDM method should attain such a wide range of accuracy for different values of J.

The differences in the DQG solution accuracy between magic and nonmagic angular momentum values suggest that there might exist a qualitative difference in the electronic structure of the magic quantum dots versus their nonmagic counterparts. Table I supports this contention, displaying the occupation numbers for the first five natural orbitals of the low-field system described above at several characteristic values of J, where the natural orbitals are the eigenfunctions of the 1RDM. The dot exhibits greater correlation with increasing J; however, the nonmagic dots are individually much more correlated than a magic dot of similar angular momentum. In fact, at nonmagic J, the systems are so correlated that most electronic structure methods would encounter difficulty obtaining accurate energies. Variational 2RDM methods, however, usually avoid this pitfall because they do not use a Hartree-Fock reference determinant, and in general, they yield accurate results even in the presence of multireference correlation effects. As will be developed below, the difference in DQG accuracy at magic and nonmagic J is related to the fact that "ground states" at high J are effectively excited states of the total dot. The high-lying excited wave functions cannot be directly orthogonalized to the lower-lying wave functions. Orthogonality must be enforced indirectly via the approximate J-representability conditions. The high degree of correlation in combination with the approximate J-representability conditions is most likely responsible for the greater difficulty at nonmagic J.

Away from the magic angular momenta values, where electron correlation is strong, the accuracy of the variational

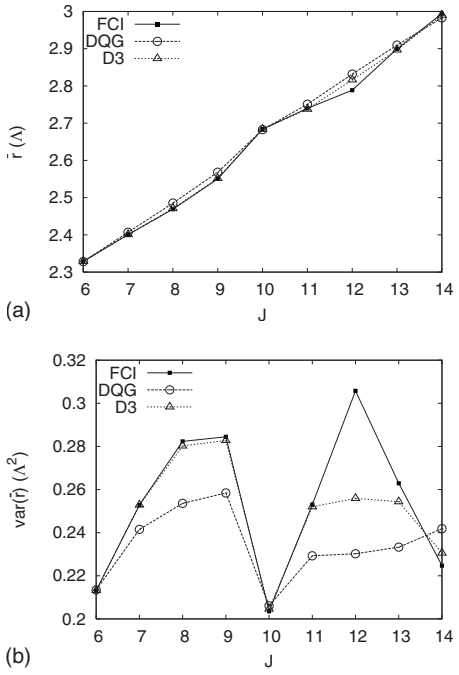

FIG. 2. (a) Average radial distance $\bar{r}=\langle|\mathbf{r}|\rangle$ of the electron from the center of the dot for four electrons at $B=2.0$ T, in units of Λ. The behavior at 10.0 T is similar but shifted downward by about $\Lambda/4$ because the increased field strength compresses the lateral extent of the dot. At magic J, the RDM solutions approximate the true $\bar{r}$ well; otherwise, they tend to overestimate $\bar{r}$, suggesting they are underestimating the correlation in the dot. (b) Variance in $\bar{r}$, in units of Λ^2. For the true wave function, the var($\bar{r}$) changes dramatically between magic and nonmagic J and reaches local minima at the magic J. The variance in the RDM solutions also achieve minima at magic J but experience a reduced range across all J.

RDM energy can be improved by including partial three-positivity. In particular, we augment the positivity of the different representations of the 2RDM by requiring ^3D to be positive semidefinite as well; we denote solutions obtained via these constraints by D3 (cf. Fig. 1). For the four electron system, D3 recovers about 102% of the correlation energy at low field, and is nearly exact at high magnetic field over the first magic period. On the interval $10<J<14$, D3 obtains an average of 144% of correlation at $B=2.0$ T and an average of 146% of correlation at $B=10$ T.

Imposition of partial three-positivity improves the accuracy (measured with respect to the energy) of the variational RDM solution, although the amount of improvement is much more substantial from $6<J<10$ than from $10<J<14$. To shed more light on this difference, we computed the average radial displacement of one electron in the dot $\bar{r}=\langle|\mathbf{r}|\rangle$ and its variance $\mathrm{var}(\bar{r})=\langle|\mathbf{r}|^2\rangle-\langle|\mathbf{r}|\rangle^2$. These values are plotted in Figs. 2(a) and 2(b), respectively, for $B=2.0$ T. As expected, the trend is for $\bar{r}$ to increase with J because the delocalization (or average radius) of the basis states $|n,l\rangle$ increases with l. The variance of $\bar{r}$ is substantially lower at magic J than at nonmagic J, which suggests that the electrons form a more coherent ring structure (i.e., all electrons at about the same radial displacement) at magic J, which agrees with the heuristic picture of magic angular momentum states in quantum

dots given earlier. The accuracy of the 2RDM values for $\bar{r}$ and var($\bar{r}$) mirrors the energy; at the magic J values, both DQG and D3 solutions exhibit enhanced accuracy relative to nonmagic J. In fact, over the first magic period, the D3 solution is nearly exact, especially for $\bar{r}$. At nonmagic J, the variational RDM solutions tend to overestimate $\bar{r}$, essentially spreading the electrons out too far from the center of the dot, and underestimate the variance.

The angular-momentum distinctions between magic and nonmagic J can be further appreciated through calculation of the pair-correlation function

$$P(\mathbf{r},\mathbf{r}_0)=\frac{(2\pi\Lambda^2)^2}{N(N-1)}\left\langle\sum_{i\neq j}\delta(\mathbf{r}_i-\mathbf{r})\delta(\mathbf{r}_j-\mathbf{r}_0)\right\rangle, \qquad (23)$$

which describes the probability of finding an electron at $\mathbf{r}$ given that one electron is at $\mathbf{r}_0$. The expectation value is taken with respect to the ground-state wave function for a given angular momentum value. We choose $\mathbf{r}_0$ fixed along the x axis at $\bar{r}$. Pair-correlation functions are plotted in Fig. 3, again for four electrons but at $B=25$ T. The stronger field is chosen here in order to compress the lateral extent of the dot (i.e., the stronger field increases the effective confinement potential Ω and decreases Λ) and sharpen the spatial resolution of the pair-correlation plots; however, the qualitative behavior with respect to the accuracy of the DQG solution is the same as at weaker field strengths. Figure 3 reveals key symmetry differences in the FCI wave function between magic and nonmagic angular momenta that are not captured by the DQG solution. At magic $J=10$ and 14, the FCI wave function has fourfold symmetry, which agrees with our understanding of the origin of magic angular momenta [58–60]. These features are reproduced by the DQG solution, and the corresponding DQG energy is a good approximation to the FCI result: 102 and 108 % of correlation for $J=10$ and $J=14$, respectively. Away from the magic values, the FCI solutions apparently have threefold symmetry, suggesting the remaining electron is centered at the origin. On the other hand, the DQG result retains the same fourfold symmetry as at the magic angular momenta. Therefore, diminished accuracy of the DQG energy relative to FCI at these J values is not surprising; the DQG result obtains 174% of correlation at $J=13$ and 150% of correlation at $J=15$.

Differences in the accuracy of DQG, D3 and higher-constrained RDM solutions between magic and nonmagic J values is not unique to four-electron systems. Figure 4 displays the FCI energy as a function of J for five electrons at $B=2.0$ T, along with the DQG and D3 solutions. In addition, we investigate the next level of partial three-positivity conditions by augmenting the positivity of the ^2D, ^2Q, and ^2G matrices with the positivity of ^3D and ^3Q (denoted D3Q3). As before, the accuracy of the DQG solution is excellent at the magic angular momentum values $J=10$ and 15, achieving about 110% of the correlation energy in both cases. Away from the magic angular momenta, the shortcomings of the DQG solution is remedied by the application of stronger positivity conditions. In particular, D3Q3 positivity maintains consistent accuracy across the entire magic period $10<J<15$ of about 105% of correlation, with enhanced accuracy (as good as 101%) at the magic values.

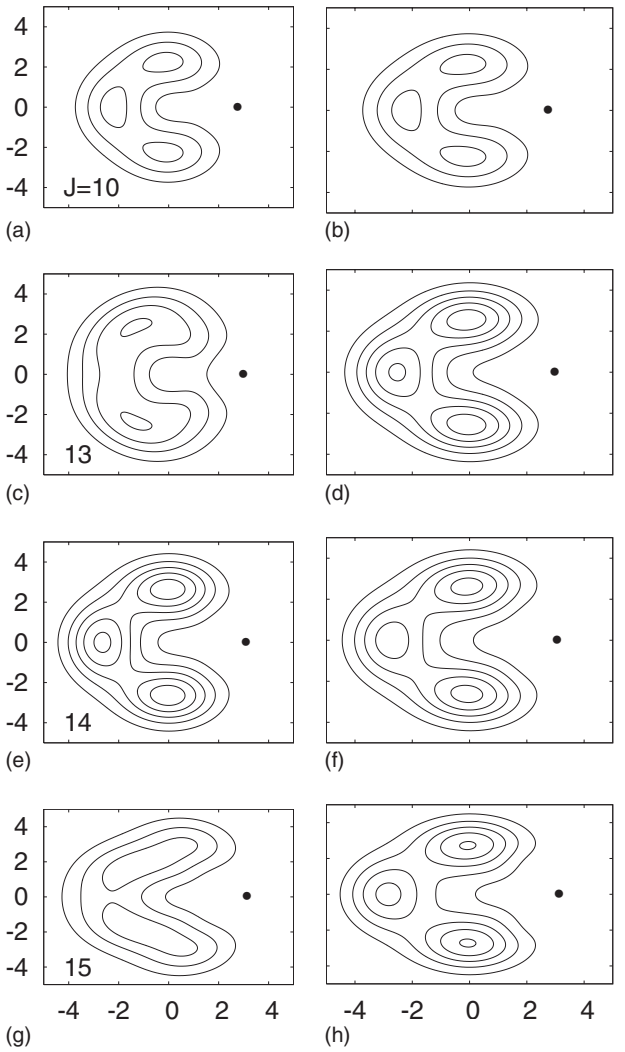

FIG. 3. The exact (FCI) and two-positivity (DQG) pair-correlation functions $P(\mathbf{r},\mathbf{r}_0)$ are plotted in the left and right columns, respectively, for four electrons at magic ($J=10,14$) and nonmagic ($J=13,15$) angular momentum values. Both the x and y axes are in units of Λ. Each plot shows probability contours for finding an electron given that a second electron is located at the indicated dot, with $\mathbf{r}_0=\bar{r}$. At the magic angular momenta, the symmetry of the DQG solution mirrors the exact wave function; both have fourfold symmetry about the origin. At nonmagic J, the FCI solutions apparently have threefold rotational symmetry, but the DQG solution maintains the fourfold symmetry of the magic solutions. The pair correlation functions explain the differences in the accuracy of the DQG solution between magic and nonmagic angular momenta values (cf. Fig. 1).

As in the four-electron system, we suspect the deficiencies in the DQG solution's accuracy at nonmagic angular momentum is related to a symmetry difference between the FCI wave function and the RDM solution. Exact (FCI) and variationally determined pair correlation functions for the five-electron dot at $B=25$ T are shown for a magic angular momentum value ($J=15$) in Fig. 5(a) and for a nonmagic angular momentum ($J=18$) in Fig. 5(b). When $J=15$, both

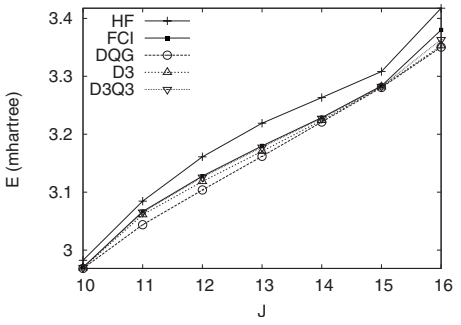

FIG. 4. Ground-state energy as a function of J for five electrons at $B=2.0$ T. Augmenting standard two-positivity by the positivity of both ^3D and ^3Q (denoted D3Q3), the variational minimization accurately reproduced the FCI energy over the first magic period $10<J<15$.

the FCI wave function and the DQG solution exhibit fivefold symmetry about the center of the dot. Thus the variational procedure approaches the true wave function in this case. Away from the magic angular momentum, the FCI wave function appears to have only fourfold symmetry. The symmetry of the DQG solution for $J=18$ is not immediately clear from the figure, but appears to display the same fivefold symmetry as in the $J=15$ case. By enhancing the N-representability conditions to include partial three-positivity, the D3Q3-constrained RDM exhibits roughly the fourfold symmetry of the exact solution. As expected, when strong positivity conditions are applied to the variational procedure, the additional N-representability helps ensure the resulting solution has the proper symmetry.

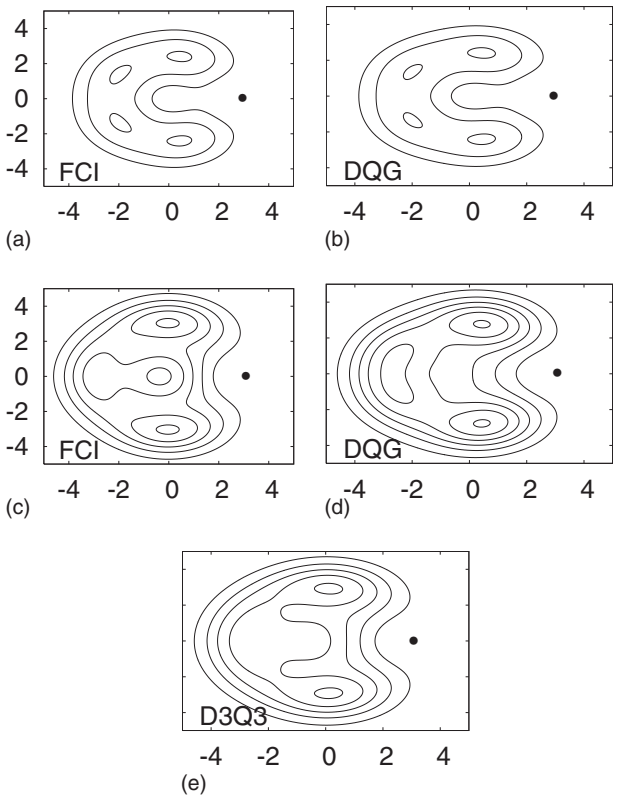

FIG. 5. Pair correlation functions for a five-electron dot at $B=25.0$ T. Both axes are calibrated in units of Λ. (a),(b) FCI (left) and DQG (right) plots for the $J=15$ magic angular momentum dot. In this case, the variational procedure identifies a solution of the correct symmetry. (c)–(e) FCI (left), DQG (right), and D3Q3 (bottom) plots for the $J=18$ nonmagic angular momentum dot. In this case, the exact solution demonstrates fourfold symmetry about the central axis. The symmetry of the DQG solution is not immediately obvious but appears to be fivefold. The enhanced positivity of D3Q3 brings the pair correlation function back to something that closely resembles the fourfold symmetry of the exact solution.

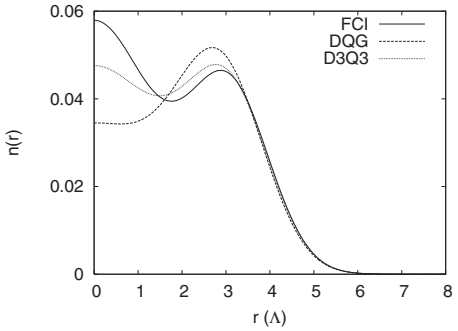

FIG. 6. Radial electron density plots for the five-electron quantum dot at nonmagic $J=18$. The solid curve indicates the FCI wave function while the dashed line indicates the DQG solution. The curves describe different densities. In particular, the FCI curve has two peaks, indicating one electron at the center of the dot and the rest at approximately 3Λ, while the DQG curve only shows one peak in the radial electron density. Imposition of partial three-positivity (D3Q3, dotted line) recovers a solution with two peaks in the radial change density. This plot sheds light on the different pair correlation functions shown in Fig. 5(b).

The symmetry differences between the wave functions in Fig. 5(b) may be further understood by examining the radial charge density $n(r)$ defined by

$$n(r) = \frac{N}{(2\pi\Lambda^2)^2} \int P(\mathbf{r},\mathbf{r}_0) d\mathbf{r}_0. \tag{24}$$

The angular momentum blocking of ^2D ensures that $n(r)$ contains no angular information, so it is a measure of the radial electron density in the dot. Figure 6 shows $n(r)$ for the FCI, DQG, and D3Q3 wave functions at the nonmagic angular momentum value $J=18$, again at the stronger field $B=25$ T to correspond with the pair correlation functions in Fig. 5(b). The FCI radial charge density here displays two distinct peaks, indicating a wave function with one centrally localized electron surrounded by a ring of $N-1$ electrons [59]. However, the DQG radial charge density more closely resembles a system with only one peak, indicating all electrons at roughly the same distance from the center of the dot. The plot more clearly confirms what was suggested in Fig. 5(b); namely, that DQG positivity is not strong enough in this case to recover the spatial symmetry of the true wave function. Turning to D3Q3 positivity, the radial charge density again displays a two-peak structure. The added strength of the partial three-positivity means that the optimized RDM reflects the symmetry of the true wave function, and as a result about 103% of the correlation energy is recovered.

Finally, it is important to point out that the performance of variational RDM theory for quantum dots is not unique to the four- and five-electron systems detailed above. In particular, we computed energy spectra for $N=6$ and 8, although computational considerations prevent the tabulation of large quantities of data for these higher number of electrons. In general, we found that energy disparity between magic and nonangular momenta for DQG positivity tended to increase with N. Stronger positivity conditions (such as the D3Q3 condition or the more expensive T2 condition [52]) bring the accuracy of the variational RDM method in these systems in line with the smaller systems described above, typically within 120% of the correlation energy.

V. CONCLUSIONS AND FUTURE WORK

In this paper, we applied variational 2RDM techniques to spinless, N-electron, interacting quantum dots to compute a spectrum of energies and 2RDMs, where each energy and 2RDM corresponds to a distinct value of the orbital angular momentum J. We found that the accuracy of the resulting solution is highly dependent upon the spatial symmetry of the wave function and the total orbital angular momentum J. At certain magic values J_m, the wave function possesses high rotational symmetry that is captured by the two-positivity constraints. Away from the magic values, the wave function is much more correlated and often exhibits different spatial symmetry that is not recovered by the two-positivity conditions. In these cases, imposition of stronger positivity conditions often results in an optimized 2RDM of the proper rotational symmetry, with a correspondingly more accurate energy.

While a single strength of positivity conditions does not render uniform accuracy across a range of J for a given system, it is important to remember that, except for the lowest energy of the spectrum, the J states with higher energies are essentially excited states. In the 2RDM calculations the 2RDMs implicitly represent wave functions whose orthogonality is being enforced solely by J-representability conditions, which are necessary and sufficient only in the limit of complete N-representability conditions. In the presence of strong multireference correlation at nonmagic J, the two-positivity conditions in combination with the J-representability conditions are not sufficiently stringent to prevent the solutions from exhibiting a rotational symmetry different from the full CI solutions. As additional N-representability conditions such as partial three-positivity constraints are added, however, both the energies and rotational symmetries at nonmagic J approach those from CI. The difficulty of nonmagic J is not necessarily a serious limitation for three reasons. (i) Because of the strong multireference correlation, the nonmagic J states will be difficult to treat with any electronic structure methods other than full CI. (ii) The overall ground state for a dot with a given number of particles occurs at a single J, always magic. (iii) Because the magic J are local minima in the electronic spectrum, laboratory studies with quantum dots almost always involve a magic angular momentum state, and since simple two-positivity performs well in these cases, 2RDM theory can be a useful tool for benchmarking the electronic structure of these systems.

The question remains if there is a way to make a reduced density matrix calculation more cognizant of the quantum dot's N-particle rotational symmetry. On possibility is to exploit a hidden symmetry of the quantum-dot Hamiltonian that is related to and yet distinct from the angular momentum symmetry. For a many-electron quantum-dot Hamiltonian the parabolic confinement potential possesses the unique property that center-of-mass (c.m.) motion separates from the remainder of the Hamiltonian (i.e., the relative motion), resulting in a total wave function that factors into c.m. and relative motion terms [44]. By a clever change of representation, other authors have employed c.m. symmetry to reduce the configuration space of large-scale CI calculations on quantum dots [21,61,62]. We speculate that making the same change of representation and constraining the expectation value of collective-motion operators in the variational calculation may result in enhanced accuracy for all (magic and nonmagic) values of J, even at the two-positivity level. An alternate approach to exploiting the c.m. separability would be to employ a rotating frame for the quantum-dot Hamiltonian [63] and perform a variational calculation only on the relative-motion orbitals.

Variational RDM techniques were successfully applied to interacting electrons under parabolic confinement. The systems exhibit much greater electronic correlation than typical molecules with similar numbers of electrons. Both larger basis sets and higher symmetries were employed for the dots than for corresponding atoms and molecules. Simple properties of the quantum dots were calculated to examine the structure of the optimized 2RDM relative to the 2RDM computed through a FCI calculation. At magic angular momentum values, two-positivity conditions are sufficient to recover accurate energies and properties. Away from these magic values, stronger positivity conditions are needed to recover solutions of comparable accuracy. Advantages of the variational 2RDM method for dots, which can be further developed, include: (i) lower bounds on the energies for all J values, (ii) polynomial-time calculation of approximate 2RDMs without wave functions, (iii) exploitation of angular symmetry in the sparse block-diagonal structure of the 2RDM, (iv) accurate description of multireference correlation (entanglement) effects, and (v) direct calculation of one- and two-electron properties from the 2RDM. Application of variational RDM techniques to a new class of quantum-mechanical systems demonstrates the versatility of reduced density matrix mechanics in the study of correlated electron systems.

ACKNOWLEDGMENTS

A.E.R. gratefully acknowledges support from the NSF. D.A.M. acknowledges the NSF, the ACS Petroleum Research Fund, Microsoft Corporation, the David and Lucile Packard Foundation, and the Henry-Camille Dreyfus Foundation for generous support.

[1] R. C. Ashoori, Nature (London) **379**, 413 (1996).
[2] C. Simon, Y.-M. Niquet, X. Caillet, J. Eymery, J.-P. Poizat, and J.-M. Gerard, Phys. Rev. B **75**, 081302(R) (2007).
[3] J. Kyriakidis and G. Burkard, Phys. Rev. B **75**, 115324 (2007).
[4] S. M. Reimann and M. Manninen, Rev. Mod. Phys. **74**, 1283 (2002).
[5] V. Fock, Z. Phys. **47**, 446 (1928).
[6] C. G. Darwin, Proc. Cambridge Philos. Soc. **27**, 86 (1930).
[7] P. A. Maksym and T. Chakraborty, Phys. Rev. Lett. **65**, 108 (1990).
[8] P. A. Maksym and T. Chakraborty, Phys. Rev. Lett. **65**, 108 (1990).
[9] P. A. Maksym and T. Chakraborty, Phys. Rev. B **45**, 1947 (1992).
[10] D. Pfannkuche, V. Gudmundsson, and P. A. Maksym, Phys. Rev. B **47**, 2244 (1993).
[11] B. A. McKinney and D. K. Watson, Phys. Rev. B **61**, 4958 (2000).
[12] B. S. Kandemir, Phys. Rev. B **72**, 165350 (2005).
[13] O. Ciftja and M. G. Faruk, Phys. Rev. B **72**, 205334 (2005).
[14] F. V. Prudente, L. S. Costa, and J. D. M. Vianna, J. Chem. Phys. **123**, 224701 (2005).
[15] O. Ciftja and A. Anil Kumar, Phys. Rev. B **70**, 205326 (2004).
[16] M. Taut, J. Phys. A **27**, 1045 (1994).
[17] W. Xie, Solid State Commun. **127**, 401 (2003).
[18] F. Bolton, Solid-State Electron. **37**, 1159 (1994).
[19] A. Harju, J. Low Temp. Phys. **140**, 181 (2005).
[20] M. Koskinen, J. Kolehmainen, S. M. Reimann, J. Toivanen, and M. Manninen, Eur. Phys. J. D **9**, 487 (1999).
[21] A. Wensauer, M. Korkusiński, and P. Hawrylak, Solid State Commun. **130**, 115 (2004).
[22] R. D. Muhandiramge and J. B. Wang, Int. J. Quantum Chem. **106**, 27 (2006).
[23] *Reduced-Density-Matrix Mechanics: With Application to Many-Electron Atoms and Molecules*, edited by D. A. Mazziotti, Advances in Chemical Physics Vol. 134 (Wiley, New York, 2007).
[24] D. A. Mazziotti, Phys. Rev. A **75**, 022505 (2007).
[25] D. A. Mazziotti, in *Reduced-Density-Matrix Mechanics: With Application to Many-Electron Atoms and Molecules*, edited by D. A. Mazziotti, Advances in Chemical Physics Vol. 134 (Wiley, New York, 2007).
[26] D. A. Mazziotti, J. Chem. Phys. **126**, 184101 (2007).
[27] D. A. Mazziotti, Phys. Rev. A **76**, 052502 (2007).
[28] F. Colmenero, C. Perez del Valle, and C. Valdemoro, Phys. Rev. A **47**, 971 (1993).
[29] F. Colmenero and C. Valdemoro, Phys. Rev. A **47**, 979 (1993).
[30] H. Nakatsuji and K. Yasuda, Phys. Rev. Lett. **76**, 1039 (1996).
[31] K. Yasuda and H. Nakatsuji, Phys. Rev. A **56**, 2648 (1997).
[32] D. A. Mazziotti, Phys. Rev. A **57**, 4219 (1998).
[33] D. A. Mazziotti, Int. J. Quantum Chem. **70**, 557 (1998).
[34] D. Mukherjee and W. Kutzelnigg, J. Chem. Phys. **114**, 2047 (2001).
[35] M. Nakata, H. Nakatsuji, M. Ehara, M. Fukuda, and K. Nakata, J. Chem. Phys. **114**, 8282 (2001).
[36] D. A. Mazziotti, Phys. Rev. A **65**, 062511 (2002).
[37] Z. Zhao, B. J. Barrams, M. Fukuda, and M. L. Overton, J. Chem. Phys. **120**, 2095 (2004).
[38] D. A. Mazziotti, Phys. Rev. Lett. **93**, 213001 (2004).
[39] D. A. Mazziotti, J. Chem. Phys. **121**, 10957 (2004).
[40] E. Cancès, G. Stoltz, and M. Lewin, J. Chem. Phys. **125**, 064101 (2006).
[41] G. Gidofalvi and D. A. Mazziotti, J. Chem. Phys. **126**, 024105 (2007).
[42] D. A. Mazziotti, J. Phys. Chem. A **111**, 12635 (2007).
[43] G. Gidofalvi and D. A. Mazziotti, J. Chem. Phys. **122**, 194104 (2005).
[44] T. Chakraborty, *Quantum Dots: A Survery of the Properties of Artifical Atoms* (Elsevier, New York, 1999).
[45] L. Landau, Z. Phys. **64**, 629 (1930).
[46] D. T. Haar, Rep. Prog. Phys. **24**, 304 (1961).
[47] A. J. Coleman and V. I. Yukalov, *Coulson's Challenge*, Lecture Notes in Chemistry Vol. 72 (Springer, Berlin, 2000).
[48] A. J. Coleman, Rev. Mod. Phys. **35**, 668 (1963).
[49] J. von Neumann, *Mathematical Foundations of Quantum Mechanics* (Princeton University Press, Princeton, NJ, 1995).
[50] C. Garrod and J. Percus, J. Math. Phys. **5**, 1756 (1964).
[51] D. A. Mazziotti and R. M. Erdahl, Phys. Rev. A **63**, 042113 (2001).
[52] D. A. Mazziotti, Phys. Rev. A **74**, 032501 (2006).
[53] A. Szabo and N. S. Ostlund, *Modern Quantum Chemistry: Introduction to Advanced Electronic Structure Theory* (Dover, New York, 1982).
[54] R. M. Erdahl, Int. J. Quantum Chem. **13**, 697 (1978).
[55] S. Fraga and F. W. Birss, Theor. Chim. Acta **5**, 398 (1966).
[56] N. Björnå, J. Phys. B **4**, 424 (1971).
[57] G. Gidofalvi and D. A. Mazziotti, Phys. Rev. A **72**, 052505 (2005).
[58] P. A. Maksym, Physica B **184**, 385 (1993).
[59] T. Sedi, Y. Kuramoto, and T. Nishino, J. Phys. Soc. Jpn. **65**, 3945 (1996).
[60] W. Y. Ruan, Y. Y. Liu, C. G. Bao, and Z. Q. Zhang, Phys. Rev. B **51**, 7942 (1995).
[61] P. Hawrylak and D. Pfannkuche, Phys. Rev. Lett. **70**, 485 (1993).
[62] P. Hawrylak, Phys. Rev. Lett. **71**, 3347 (1993).
[63] P. A. Maksym, Phys. Rev. B **53**, 10871 (1996).